Study of the Ridge-Loaded Helical-Groove Slow-Wave Structure

Wenxiang Wang, Guofen Yu, and Yanyu Wei

***Abstract*—The proposition to name the helical waveguide with the inner wall removed *helical groove* is presented in this paper. As an all-metal slow-wave circuit, the ridge-loaded helical-groove structure is especially suited for use in millimeter TWT's due to its advantages of large size, high manufacturing precision, and good heat dissipation. However, the analysis of this slow-wave circuit was never before done. For analyzing this structure, the cylindrical coordinates are employed in the center space and the helical ones are used in the gap and groove regions. Making use of the matching conditions of the RF fields and the continuity of the voltage and current at the boundaries, the expressions for the dispersion and the coupling impedance of the ridge-loaded helical groove are obtained. The relationship of the dispersion and impedance to the ridge dimensions are also given. It is indicated from the calculation results that approximately 30% bandwidth for this structure can be achieved.**

***Index Terms*—Millimeter wave, slow-wave structure, traveling-wave tube.**

I. Introduction

As THE component of beam-wave interaction of a TWT for exciting microwave energy, the slow-wave circuit directly influences the TWT's properties. A helix and its modifications (ring-bar, ring-loop structures, etc.) and coupled-cavity (and ladder line, etc.) are most commonly used in TWT's as slow-wave structures. A helix has very wide bandwidth, but the small thermal capacity, and the low heat dissipation are its fatal weaknesses, which restrict the output power of TWT's. The thermal dissipation capability of the coupled cavity is clearly better than that of the helix; however, its operation bandwidth is considerably more narrow compared with that of the helix.

Seeking some new slow-wave structures possessing broader bandwidth and higher power capacity is the constant goal for which the microwave tube workers make their great efforts. It seems difficult to satisfy both excellent properties simultaneously. This problem is to some extent linked to the openness of the slow-wave system: weaker dispersion and wider bandwidth require an increase in the openness within certain dimensional range; conversely, improving heat dissipation and enhancing the power level require more closeness. It is thus clear that the two requirements above are conflicting. Consequently, up to now the efforts are mainly concentrated on further increasing the output power of a helix TWT by means of new techniques, new materials, new processes, and on searching for some new all-metal slow-wave structures which have wider bandwidth—such as helical waveguide, helical groove, π-type line, etc.

Manuscript received August 15, 1996; revised June 20, 1997.

The authors are with the Institute of High Energy Electronics, University of Electronic Science and Technology of China, Chengdu, Sichuan 610054, China.

Publisher Item Identifier S 0018-9480(97)07103-2.

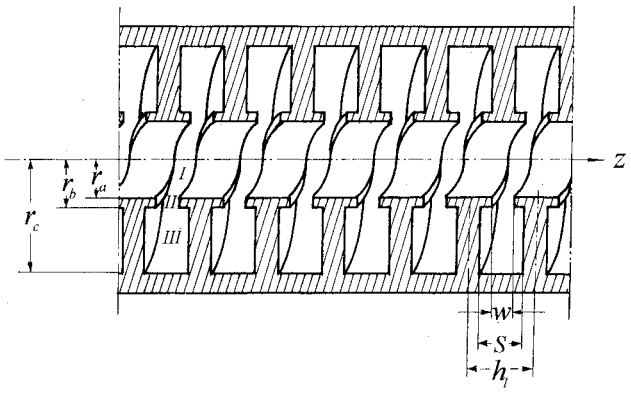

Fig. 1. The configuration of the ridge-loaded helical-groove slow-wave circuit.

The configuration of a helical-groove slow-wave structure is shown in Fig. 1. This kind of slow-wave circuit is usually named *helical waveguide*, but this leads to some confusion because the structure formed by directly spiraling a rectangular waveguide about an axis into a helix is also called a helical waveguide [1]. The helical groove can be considered as being formed by removing the inner wall of the helical waveguide; however, a large difference exists between them when they are used as the slow-wave circuit. An annular electron beam or multibeam injects axially through a slit gap (or some holes) at the waveguide's broadwall in the case of a helical waveguide structure [2] and the electron-beam passageway is the central hole on the axis in the case of the helical-groove structure. Thus, in order to avoid ambiguity and tally with the actual situation, it is reasonable to name the latter *helical groove*.

The characteristics of the helical groove are as follows. The dimension precision can be easily ensured in the manufacturing and machining. The large power-handling capability can be achieved owing to the all-copper structure. Large sizes, low cost, high precision, and good heat dissipation make the helical groove slow-wave system especially suitable for use in millimeter TWT's.

The original concept of the helical groove may be traced back to 1949. In that year, Field presented the proposal of using the helical groove as the slow-wave system [3]. Afterwards, the analyses of rectangular helical-groove structure were done by Henoch [4] and Nwachuku [5]. The studies of this structure were also developed in the USSR [6]. In Henoch's work, the TE and TM modes and their space

harmonics are considered in the center region of the helical groove, in the groove space the TE mode propagating in the helical direction and the helical coordinates are employed. Henoch's theory is improved by Fould [7], who theorized that the fast-wave and slow-wave modes are simultaneously taken into account and the dispersion equation of the loadless helical groove is obtained under the condition of pitch angle ψ satisfying $\tan^2\psi \ll 1$.

The Raytheon Company reported at the International Electron Devices Meeting (IEDM'88) that an experimental millimeter-wave TWT using a ridge-loaded helical groove as a slow-wave circuit had been built [8]. This TWT obtained output power of 163 W at 42 GHz with an electronic efficiency of 6.2%. The report noted that none of the existing theories of the helical-groove structure are capable of analyzing the effects of the ridge dimensions on circuit characteristics, though the results of cold-test experiments and TWT's parameters are given in Raytheon's paper.

In this paper, using the matching conditions which are simpler than that employed in Henoch's and Fould's theories, and considering the effects of the ridge load, we obtained the dispersion equation and the coupling impedance expression of the ridge-loaded helical-groove circuit and numerically calculated the relationships of the dispersion and coupling impedance versus ridge dimensions. This paper includes six sections. Section I includes the proposal for the name of helical groove. Section II gives the field distributions in the structure and the conversion between center-space and groove-space coordinates. In Section III, the dispersion characteristic is derived by using boundary conditions, particularly, the voltage and current continuity on the outer surface of the ridges. The solution of the interaction impedance is presented in Section IV. Section V gives the numerical results. Finally, a short conclusion is given in Section VI.

II. The Fields in the Helical Groove Structure

A. The Coordinate Systems

Fig. 1 gives the longitudinal section through the axis of the ridge-loaded helical-groove slow wave circuit model. The azimuthal coordinate of this section is ϕ. In this figure, h_l, s, and w represent the structure period, groove width, and gap breadth, respectively; r_a, r_b, and r_c indicate the radii of the center space, outer surface of the ridge, and the groove bottom, respectively. The analytic model can be divided into the following three regions:

Region I interaction regions, i.e. center space $0 \le r \le r_a$;
Region II gap space $r_a \le r \le r_b, (m+\phi/2\pi)h_l - w/2 \le z \le (m+\phi/2\pi)h_l + w/2$;
Region III groove space $r_b \le r \le r_c$, $(m+\phi/2\pi)h_l - s/2 \le z \le (m+\phi/2\pi)h_l + s/2$

where m is the order of the groove or gap. In Region I, the cylindrical coordinates r, ϕ, z are employed and the helical coordinates r, θ, ξ are used in Regions II and III. Both coordinate systems on the surface r_a are shown in Fig. 2. Obviously, the helical coordinates are not an orthogonal system because the θ direction is along the center line of the groove. However, if the pitch angle is small enough that the condition $\tan^2\psi \ll 1$ can be satisfied, it does approximate to a cylindrical coordinate system. Then, the θ will be measured in the direction being perpendicular to the axis, but not along the helical direction of the groove, and the ξ will be approximately equal to z.

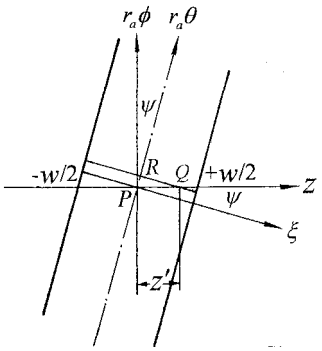

Fig. 2. The coordinate systems on surface $r = r_a$.

B. The Fields in Interaction Region

The combination of TE and TM waves may exist in the center space, and both slow and fast waves may be excited in the same region due to the closeness of the structure. Each of these waves will consist of infinite sums of space harmonics as a result of the periodicity of the structure. Thus, we have the following fields in Region I:

$$\begin{cases} E_z^{\mathrm{I}} = \sum_{n=-\infty}^{\infty} A_n^{\mathrm{I}} \gamma_n^2 F_n(\gamma_n r) e^{j(n\phi-\beta_n z)} \\ E_r^{\mathrm{I}} = \pm j \sum_{n=-\infty}^{\infty} [A_n^{\mathrm{I}} \gamma_n \beta_n F_n'(\gamma_n r) \\ \quad -B_n^{\mathrm{I}}(n\omega\mu_0/r) F_n(\gamma_n r)] e^{j(n\phi-\beta_n z)} \\ E_\phi^{\mathrm{I}} = \mp \sum_{n=-\infty}^{\infty} [A_n^{\mathrm{I}}(n\beta_n/r) F_n(\gamma_n r) \\ \quad -B_n^{\mathrm{I}} \omega\mu_0 \gamma_n F_n'(\gamma_n r)] e^{j(n\phi-\beta_n z)} \\ H_z^{\mathrm{I}} = j \sum_{n=-\infty}^{\infty} B_n^{\mathrm{I}} \gamma_n^2 F_n(\gamma_n r) e^{j(n\phi-\beta_n z)} \\ H_r^{\mathrm{I}} = \pm \sum_{n=-\infty}^{\infty} [A_n^{\mathrm{I}}(nk^2/r\omega\mu_0) F_n(\gamma_n r) \\ \quad -B_n^{\mathrm{I}} \gamma_n \beta_n F_n(\gamma_n r)] e^{j(n\phi-\beta_n z)} \\ H_\phi^{\mathrm{I}} = \pm j \sum_{n=-\infty}^{\infty} [A_n^{\mathrm{I}}(k^2\gamma_n/\omega\mu_0) F_n'(\gamma_n r) \\ \quad -B_n^{\mathrm{I}}(n\beta_n/r) F_n(\gamma_n r)] e^{j(n\phi-\beta_n z)}. \end{cases} \tag{1}$$

If $\gamma_n^2 = \beta_n^2 - k^2 > 0$, (1) represents slow-wave modes, $F_n(\gamma_n r) = I_n(\gamma_n r)$ and uses the upper sign from the signs $\pm$ or $\mp$ in front of some expressions. If $\gamma_n^2 = k^2 - \beta_n^2 > 0$, these express fast-wave modes, $F_n(\gamma_n r) = J_n(\gamma_n r)$ and use the lower sign. I_n represents the modified Bessel function of the first kind of order n, and J_n is the ordinary Bessel function of the first kind. γ_n is the radial propagation constant, k is the wave number in free space, β_n is the axial propagation constant and can be expressed as

$$\beta_n = \beta_0 + (2n\pi/h_l) \tag{2}$$

where n is the order of the space harmonic.

C. The Fields in Gap Space and Groove Space

In the gap and groove regions, a TE mode which is homogeneous across the breadth of the gap and groove is assumed; in other words, we suppose the electric field has no

variation in the ξ direction, thus the fields can be written as

$$\begin{cases} E_\xi^{\mathrm{II,III}} = [B_v^{\mathrm{II,III}} J_{-v}(kr) - A_v^{\mathrm{II,III}} J_v(kr)] e^{-jv\theta} \\ H_r^{\mathrm{II,III}} = (v/r\omega\mu_0)[B_v^{\mathrm{II,III}} J_{-v}(kr) - A_v^{\mathrm{II,III}} J_v(kr)] e^{-jv\theta} \\ H_\theta^{\mathrm{II,III}} = -j(k/\omega\mu_0)[B_v^{\mathrm{II,III}} J'_{-v}(kr) - A_v^{\mathrm{II,III}} J'_v(kr)] e^{-jv\theta} \\ E_r^{\mathrm{II,III}} = E_\theta^{\mathrm{II,III}} = H_\xi^{\mathrm{II,III}} = 0. \end{cases} \tag{3}$$

The $J_{-v}(kr)$ should be replaced by $Y_N(kr)$ in (3) when v is an integral N. Here, v is an angular propagation coefficient and indicates the wavelength number in one revolution or the wavelength number corresponding to a 2π change of θ

$$\beta_0 h_l = 2\pi v.$$

Then

$$\beta_n = 2\pi(n+v)/h_l \tag{4}$$

and the slow-wave condition $\beta_n^2 > k^2$ can be rewritten as

$$\lambda > h_l/|n+v|. \tag{5}$$

D. The Conversion Between Coordinate Systems

The fields of Regions II and III are independent of the ξ direction in the r, θ, and ξ coordinate system, but the fields in the r, ϕ, z coordinate system will vary with z. Consequently, the expressions of the fields variation with z must be known for matching them at the surface $r = r_a$, which is parallel to the axis z but not to ξ.

As shown in Fig. 2, let us consider point P on the middle line of the groove

$$z_p = (m + \phi/2\pi)h_l.$$

The variation for θ when z changes along the axis from P to an arbitrary point Q is

$$\Delta\theta = \frac{\overline{PR}\cos\psi}{r_a} = \frac{z'\sin\psi\cos\psi}{r_a}$$

thus

$$\theta = \theta_p + \Delta\theta = (2m\pi + \phi) + \frac{z'\sin\psi\cos\psi}{r_a}. \tag{6}$$

Substituting the above expressions into (3), the relations between the fields and z are derived.

III. Dispersion Characteristic

Using the matching conditions of fields at the boundaries between regions, we can get the dispersion equation of a ridge-loaded helical-groove circuit.

A. Matching the Electric Fields at $r = r_a$

The matching conditions of E-fields at boundary $r = r_a$ are

$$\begin{cases} E_z^{\mathrm{I}} = E_\xi^{\mathrm{II}} \cos\psi \\ E_\phi^{\mathrm{I}} = -E_\xi^{\mathrm{II}} \sin\psi. \end{cases} \tag{7}$$

Substituting E_ξ^{II} in (3) and θ in (6) into (7), and applying the Fourier analysis, we obtain

$$\begin{cases} A_n^{\mathrm{I}} = \frac{w}{h_l}[B_v^{\mathrm{II}} J_{-v}(kr_a) - A_v^{\mathrm{II}} J_v(kr_a)] \frac{\cos\psi \sin(p\pi w/h_l)}{\gamma_n^2 F_n(\gamma_n r_a)(p\pi w/h_l)} \\ \pm B_n^{\mathrm{I}} = \frac{[(\pm n\beta_n/r_a) - (\gamma_n^2 \tan\psi)]}{\omega\mu_0\gamma_n^3 F'_n(\gamma_n r_a)} \frac{w}{h_l}[B_v^{\mathrm{II}} J_{-v}(kr_a) - A_v^{\mathrm{II}} J_v(kr_a)] \\ \quad \cdot \frac{\cos\psi \sin(p\pi w/h_l)}{p\pi w/h_l} \end{cases} \tag{8}$$

where

$$p = v\cos^2\psi + \mathrm{n}.$$

B. The Continuity of Magnetic Fields at $r = r_a$

The other matching condition on the boundary between Regions I and II should be the continuity for the average value of H_θ across the groove

$$\int_{(m+\phi/2\pi)h_l - w/2}^{(m+\phi/2\pi)h_l + w/2} (H_\phi^{\mathrm{I}} \cos\psi + H_z^{\mathrm{I}} \sin\psi) dz = \int_{(m+\phi/2\pi)h_l - w/2}^{(m+\phi/2\pi)h_l + w/2} H_\theta^{\mathrm{II}}\, dz. \tag{9}$$

Inserting (1), (3), (6), and (8) into (9) we have

$$\begin{aligned} &\pm \frac{w}{h_l}[B_v^{\mathrm{II}} J_{-v}(kr_a) - A_v^{\mathrm{II}} J_v(kr_a)] \\ &\quad \cdot \sum_{n=-\infty}^{\infty} \frac{k}{\gamma_n}\left[\frac{F'_n(\gamma_n r_a)}{F_n(\gamma_n r_a)} - \frac{1}{(k\gamma_n)^2} \cdot \frac{F_n(\gamma_n r_a)}{F'_n(\gamma_n r_a)} \cdot \left(\frac{n\beta_n}{r_a} \mp \gamma_n^2 \tan\psi\right)^2\right] \\ &\quad \cdot \frac{\cos^2\psi \sin(p\pi w/h_l)}{p\pi w/h_l} \frac{\sin(\beta_n w/2)}{\beta_n w/2} \\ &\quad = -[B_v^{\mathrm{II}} J'_{-v}(kr_a) - A_v^{\mathrm{II}} J'_v(kr_a)] \\ &\quad \cdot \frac{\sin(v\sin^2\psi)\pi w/h_l}{(v\sin^2\psi)\pi w/h_l}. \end{aligned} \tag{10}$$

Under the assumption $\tan^2\psi \ll 1$, we get $\sin^2\psi \ll 1$, $\cos^2\psi \approx 1$, and

$$\cos^2\psi \frac{\sin(p\pi w/h_l)}{p\pi w/h_l} \approx \frac{\sin(\beta_n w/2)}{\beta_n w/2}$$
$$\frac{\sin(v\sin^2\psi)\pi w/h_l}{(v\sin^2\psi)\pi w/h_l} \approx 1.$$

Thus, (10) can be rewritten as

$$\begin{aligned} -\frac{B_v^{\mathrm{II}} J'_{-v}(kr_a) - A_v^{\mathrm{II}} J'_v(kr_a)}{B_v^{\mathrm{II}} J_{-v}(kr_a) - A_v^{\mathrm{II}} J_v(kr_a)} &= \pm \frac{w}{h_l} \sum_{n=-\infty}^{\infty} \frac{k}{\gamma_n}\left[\frac{F'_n(\gamma_n r_a)}{F_n(\gamma_n r_a)} - \frac{1}{(k\gamma_n)^2} \cdot \frac{F_n(\gamma_n r_a)}{F'_n(\gamma_n r_a)} \cdot \left(\frac{n\beta_n}{r_a} \mp \gamma_n^2 \tan\psi\right)^2\right] \\ &\quad \cdot \left[\frac{\sin(\beta_n w/2)}{\beta_n w/2}\right]^2. \end{aligned} \tag{11}$$

C. The Boundary Condition at $r = r_c$

It is clear that at the surface $r = r_c$, the tangential E-field should be zero:

$$E_{\xi}^{\mathrm{III}} = [B_v^{\mathrm{III}} J_{-v}(kr_c) - A_v^{\mathrm{III}} J_v(kr_c)]e^{-jv\theta} = 0. \tag{12}$$

Without sacrificing the generality, we can assume

$$B_v^{\mathrm{III}} = E_0 J_v(kr_c) \tag{13}$$

and then from (12) we have

$$A_v^{\mathrm{III}} = E_0 J_{-v}(kr_c). \tag{14}$$

D. The Matching Conditions at $r = r_b$

The matching conditions for electromagnetic fields can not directly be used at the boundary between Space II and III, because only the constant E_ξ component of E-fields is considered in those regions; furthermore, the width of Regions II and III are different. Replacing the matching of the fields by the voltage and current continuity conditions at $r = r_b$ gives

$$\begin{cases} V_z^{\mathrm{II}} = V_z^{\mathrm{III}} \\ J_r^{\mathrm{II}} = J_r^{\mathrm{III}} - B_1 V_z^{\mathrm{III}} \end{cases} \tag{15}$$

where [9]

$$\begin{aligned} B_1 &= j\omega C_1 \\ C_1 &= \frac{\varepsilon}{2\pi}\left[\frac{\alpha^2+1}{\alpha}\ln\frac{1+\alpha}{1-\alpha} - 2\ln\frac{4\alpha}{1-\alpha^2}\right] \\ \alpha &= \frac{w}{s} \end{aligned}$$

provided that $s < 0.2\,\lambda$, ε is the permittivity of the vacuum, C_1 is the discontinuity capacitance at boundary $r = r_b$, and B_1 is the corresponding susceptance.

The voltage can be expressed as

$$\begin{cases} V_z^{\mathrm{II}} = E_\xi^{\mathrm{II}} w\cos\psi \\ V_z^{\mathrm{III}} = E_\xi^{\mathrm{III}} s\cos\psi \end{cases} \tag{16}$$

and the current of unit length on the surface of the conductor should be

$$\begin{cases} J_r^{\mathrm{II}} = H_\theta^{\mathrm{II}} \\ J_r^{\mathrm{III}} = H_\theta^{\mathrm{III}}. \end{cases} \tag{17}$$

By means of (3), (13), and (14), the A_v^{II}, B_v^{II} may be solved from (15) as follows:

$$\begin{cases} A_v^{\mathrm{II}} = \frac{E_0}{R_v(r_b, r_b)}\Big\{J_{-v}(kr_b)R_v(r_b, r_c) + \Big[\frac{\omega^2\mu_0}{k}J_{-v} \\ \qquad\qquad \cdot(kr_b)C_1 s\cos\psi - \frac{s}{w}\frac{J_{-v}(kr_b)J'_{-v}(kr_b)}{J_v(kr_b)} \\ \qquad\qquad - \frac{s}{w}\frac{Q_v(r_b, r_b)}{J_v(kr_b)}\Big]P_v(r_b, r_c)\Big\} \\ B_v^{\mathrm{II}} = \frac{E_0}{R_v(r_b, r_b)}\Big\{J_v(kr_b)R_v(r_b, r_c) + \Big[\frac{\omega^2\mu_0}{k}J_v(kr_b) \\ \qquad\qquad \cdot C_1 s\cos\psi - \frac{s}{w}J'_v(kr_b)\Big]P_v(r_b, r_c)\Big\} \end{cases} \tag{18}$$

where

$$\begin{aligned} P_v(x, y) &= J_v(kx)J_{-v}(ky) + J_{-v}(kx)J_v(ky) \\ R_v(x, y) &= J'_v(kx)J_{-v}(ky) - J'_{-v}(kx)J_v(ky) \\ Q_v(x, y) &= J_v(kx)J'_{-v}(ky) - J_{-v}(kx)J'_v(ky). \end{aligned}$$

E. Dispersion Equation

Inserting (18) into (11), we finally get the dispersion equation (19), shown at the bottom of the page, of the ridge-loaded helical-groove slow-wave structure.

For the circuit without ridge loading, i.e., $r_a = r_b$, $w = s$, $C_1 = 0$, the dispersion equation is reduced to

$$\begin{aligned} &\frac{R_v(r_b, r_c)}{P_v(r_b, r_c)} \\ &\quad \pm \frac{s}{h_l}\sum_{n=-\infty}^{\infty}\frac{k}{\gamma_n}\left[\frac{F'_n(\gamma_n r_b)}{F_n(\gamma_n r_b)} - \frac{1}{k^2\gamma_n^2}\frac{F_n(\gamma_n r_b)}{F'_n(\gamma_n r_b)}\right. \\ &\qquad \left.\cdot\left(\frac{n\beta_n}{r_b} \mp \gamma_n^2\tan\psi\right)^2\right]\left[\frac{\sin(\beta_n s/2)}{\beta_n s/2}\right]^2 = 0. \end{aligned} \tag{20}$$

This expression is completely identical with the results given by Fould in [7].

IV. Coupling Impedance

The coupling impedance of nth space harmonic is defined as

$$K_{cn} = \frac{E_{zn}E_{zn}^*}{2\beta_n^2 P} \tag{21}$$

where E_{zn} is the longitudinal component of the electric field of the nth space harmonic at r_e, the position of the electronic beam, and E_{zn}^* is its conjugate value. According to (1) and (8), we have

$$\begin{aligned} E_{zn}E_{zn}^* = \left(\frac{w}{h_l}\right)^2 &[B_v^{\mathrm{II}}J_{-v}(kr_a) - A_v^{\mathrm{II}}J_v(kr_a)]^2 \\ &\cdot\frac{F_n^2(\gamma_n r_e)}{F_n^2(\gamma_n r_a)}\left[\frac{\sin(\beta_n w/2)}{\beta_n w/2}\right]^2. \end{aligned} \tag{22}$$

$$\begin{aligned} &\frac{\Big\{\Big[\frac{s}{w}\frac{J'_v(kr_b)}{J_v(kr_b)} - \frac{\omega^2\mu_0}{k}C_1 s\cos\psi\Big]R_v(r_a, r_b) - \frac{s}{w}\frac{J'_v(kr_a)}{J_v(kr_b)}R_v(r_b, r_b)\Big\}P_v(r_b, r_c) -}{\Big\{\Big[\frac{s}{w}\frac{J'_v(kr_b)}{J_v(kr_b)} - \frac{\omega^2\mu_0}{k}C_1 s\cos\psi\Big]P_v(r_a, r_b) - \frac{s}{w}\frac{J_v(kr_a)}{J_v(kr_b)}R_v(r_b, r_b)\Big\}P_v(r_b, r_c) -} \\ &\frac{-R_v(r_a, r_b)R_v(r_b, r_c)}{-P_v(r_a, r_b)R_v(r_b, r_c)} \pm \frac{w}{h_l}\sum_{n=-\infty}^{\infty}\frac{k}{\gamma_n}\left[\frac{F'_n(\gamma_n r_a)}{F_n(\gamma_n r_a)} - \frac{1}{(k\gamma_n)^2}\frac{F_n(\gamma_n r_a)}{F'_n(\gamma_n r_a)}\left(\frac{n\beta_n}{r_a} \mp \gamma_n^2\tan\psi\right)^2\right] \times \left[\frac{\sin(\beta_n w/2)}{\beta_n w/2}\right]^2 = 0. \end{aligned} \tag{19}$$

P is the total power flow through the whole circuit system:

$$P = P^{\mathrm{II}} + P^{\mathrm{III}} + \sum_{n=-\infty}^{\infty} P_n^{\mathrm{I}}. \tag{23}$$

P^{II}, P^{III} are the power in Regions II and III, respectively, and P_n^{I} is the power flow of the nth space harmonic in Space I. Making use of the derived results from Section III about the components of the field, P^{I}, P^{II}, and P^{III} are as follows:

$$\begin{aligned}
&P_n^{\mathrm{I}} \\
&= \frac{1}{2}\int_0^{r_a} [E_r H_\phi^* - E_\phi H_r^*] 2\pi r\, dr \\
&= \pi r_a^2 \left(\frac{w}{h_l}\right)^2 \left[\frac{\sin(\beta_{\mathrm{n}} w/2)}{\beta_{\mathrm{n}} w/2}\right]^2 \left(\frac{\beta_n}{\omega\mu_0}\right) \\
&\cdot [B_v^{\mathrm{II}} J_{-v}(kr_a) - A_v^{\mathrm{II}} J_v(kr_a)]^2 \\
&\cdot \left\{\frac{1}{4}\left[\left(\frac{k}{\gamma_n}\right)^2 + \left(\frac{n\beta_n}{\gamma_n^2 r_a} - \tan\psi\right)^2 \left(\frac{F_n(\gamma_n r_a)}{F_n'(\gamma_n r_a)}\right)^2\right]\right. \\
&\quad \cdot \left[\frac{F_{n+1}^2(\gamma_n r_a) + F_{n-1}^2(\gamma_n r_a)}{F_n^2(\gamma_n r_a)}\right. \\
&\quad \left.\left. - \frac{F_{n+2}(\gamma_n r_a) + F_{n-2}(\gamma_n r_a)}{F_n(\gamma_n r_a)}\right] - n\frac{(\beta_n^2 + k^2)}{\gamma_n^2}\right. \\
&\quad \left. \cdot \frac{[(n\beta_n/\gamma_n^2 r_a) - \tan\psi]}{(\gamma_n r_a)(\beta_n r_a)} \frac{F_n(\gamma_n r_a)}{F_n'(\gamma_n r_a)}\right\}
\end{aligned} \tag{24}$$

$$\begin{aligned}
&P^{\mathrm{II}} \\
&= \frac{1}{2} w \int_{r_a}^{r_b} E_\xi H_r^*\, dr \\
&= \frac{1}{4}\frac{w}{\omega\mu_0}\left\{[A_v^{\mathrm{II}} J_v(kr_b) - B_v^{\mathrm{II}} J_{-v}(kr_b)]^2\right. \\
&\qquad + kr_b[A_v^{\mathrm{II}} J_{v+1}(kr_b) + B_v^{\mathrm{II}} J_{-(v+1)}(kr_b)] \\
&\qquad \times \frac{\partial}{\partial v}[A_v^{\mathrm{II}} J_v(kr_b) - B_v^{\mathrm{II}} J_{-v}(kr_b)] \\
&\qquad - kr_b[A_v^{\mathrm{II}} J_v(kr_b) - B_v^{\mathrm{II}} J_{-v}(kr_b)] \\
&\qquad \times \frac{\partial}{\partial v}[A_v^{\mathrm{II}} J_{v+1}(kr_b) + B_v^{\mathrm{II}} J_{-(v+1)}(kr_b)] \\
&\qquad - [A_v^{\mathrm{II}} J_v(kr_a) - B_v^{\mathrm{II}} J_{-v}(kr_a)]^2 \\
&\qquad - kr_a[A_v^{\mathrm{II}} J_{v+1}(kr_a) + B_v^{\mathrm{II}} J_{-(v+1)}(kr_a)] \\
&\qquad \cdot \frac{\partial}{\partial v}[A_v^{\mathrm{II}} J_v(kr_a) - B_v^{\mathrm{II}} J_{-v}(kr_a)] \\
&\qquad + kr_a[A_v^{\mathrm{II}} J_v(kr_a) - B_v^{\mathrm{II}} J_{-v}(kr_a)] \\
&\qquad \left.\cdot \frac{\partial}{\partial v}[A_v^{\mathrm{II}} J_{v+1}(kr_a) + B_v^{\mathrm{II}} J_{-(v+1)}(kr_a)]\right\}
\end{aligned} \tag{25}$$

$$\begin{aligned}
&P^{\mathrm{III}} \\
&= \frac{1}{2} s \int_{r_b}^{r_c} E_\xi H_r^*\, dr \\
&= \frac{1}{4}\frac{s}{\omega\mu_0} E_0^2 \left\{kr_b P_v(r_b, r_c)\frac{\partial}{\partial v}\right. \\
&\qquad \cdot [J_{v+1}(kr_b) J_{-v}(kr_c) + J_{-(v+1)}(kr_b) J_v(kr_c)] \\
&\qquad - kr_b[J_{v+1}(kr_b) J_{-v}(kr_c) + J_{-(v+1)} \\
&\qquad\qquad \cdot (kr_b) J_v(kr_c)] \\
&\qquad \left.\cdot \frac{\partial}{\partial v} P_v(r_b, r_c) - P_v^2(r_b, r_c)\right\}
\end{aligned} \tag{26}$$

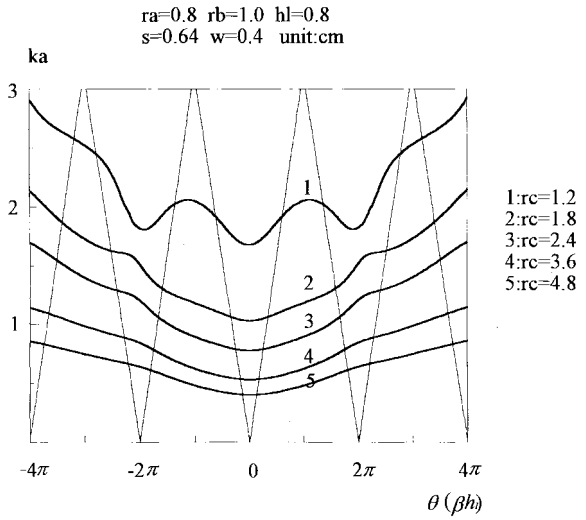

Fig. 3. The dispersion curves of the ridge-loaded helical groove with variant r_c.

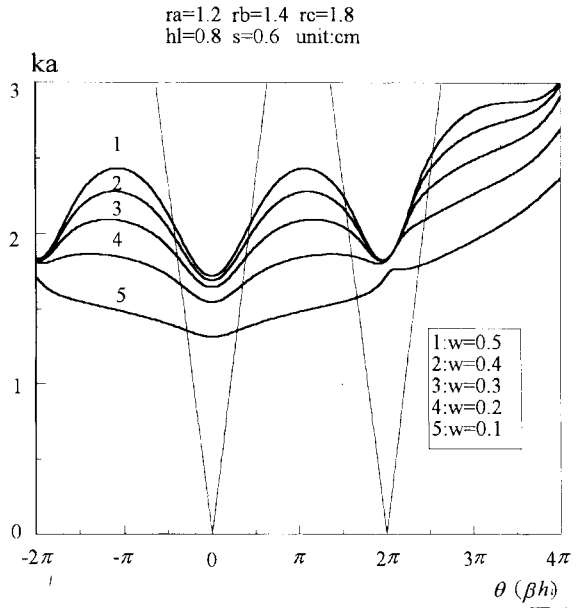

Fig. 4. The dispersion curves of the ridge-loaded helical groove with variant w.

where A_v^{II}, B_v^{II} are given by (18). If $v = N$ is a integral, then $Y_N(kr)$ should take place of $J_{-v}(kr)$, and $J_{-(v+1)}(kr)$ should be replaced by $-Y_{N+1}(kr)$. In the process of deriving P^{II} and P^{III}, the relevant integral formulas of Bessel functions from [10] were used.

V. The Results of Calculation

The dispersion curves of the fundamental mode of the ridge-loaded helical groove slow-wave structure, calculated according to (19), shown at the bottom of the previous page, are shown in Figs. 3 and 4. The lines of $\beta_n^2 = k^2$ are also given in these figures. The parts above those lines are the regions of fast waves ($k^2 > \beta_n^2$), and that below those lines are the regions of slow waves ($k^2 < \beta_n^2$). Fig. 3 shows the variations of the dispersion curves with r_c, the larger the r_c is, the lower the operation frequency and the more narrow the

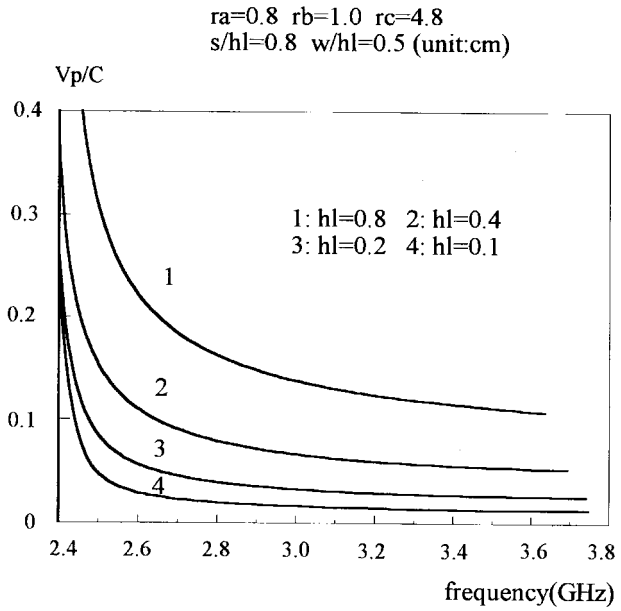

Fig. 5. The relation between phase velocity and frequency under variant h_l.

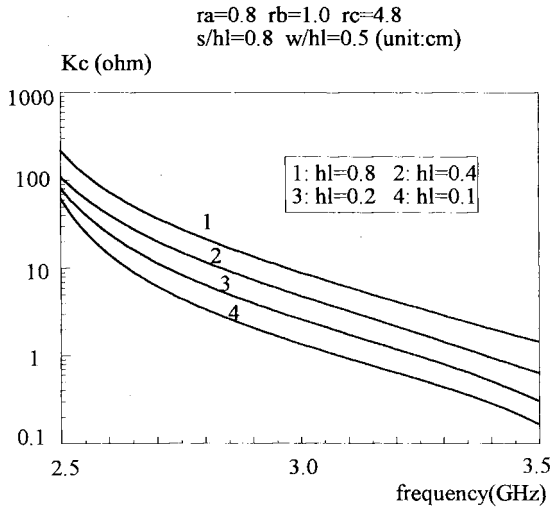

Fig. 6. The relation between coupling impedance and frequency under variant h_l.

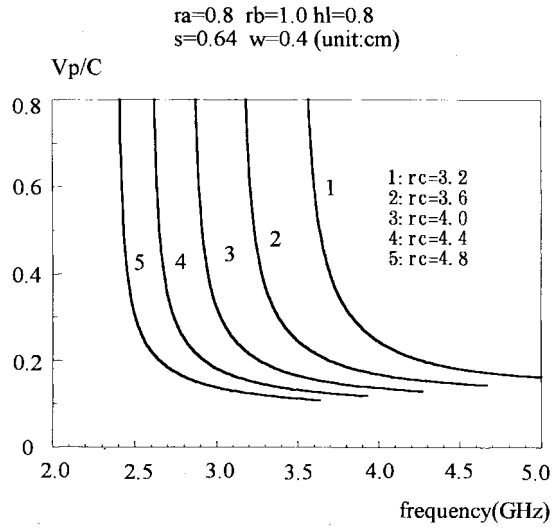

Fig. 7. The relation between phase velocity and frequency for various r_c.

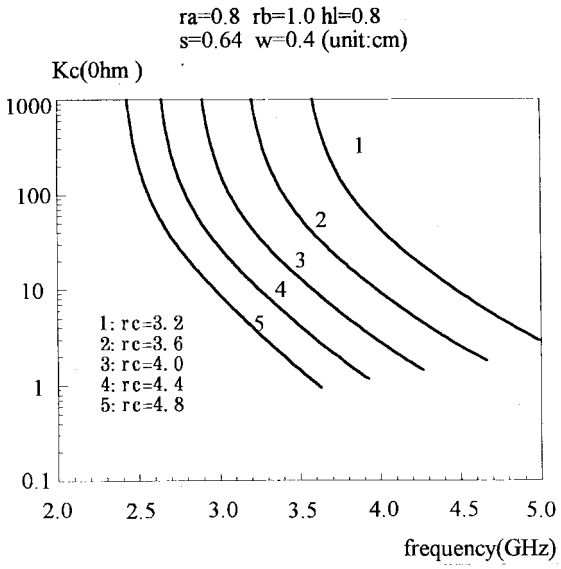

Fig. 8. The relation between coupling impedance and frequency for various r_c.

passbands are. When w, the width of the gap, is changed, the dispersion curves are shown in Fig. 4. The influence of the change of width w on the operation frequency of the helical-groove structure is not so obvious as that of the change of r_c. The bandwidth increases with the raising of w.

The dispersion curves of the high-order harmonics $(n \neq 0)$ can be obtained by moving the curves of fundamental mode by $2n\pi$ along the abscissa toward the right $(n > 0)$ or the left $(n < 0)$.

In the range of $0 < \beta_0 h_l < 2\pi$ the relations between the phase velocity or coupling impedance and the frequency for the fundamental slow wave $(\beta_n^2 > k^2)$ under various sizes of the helical grooves are shown in Figs. 5–10.

Figs. 5 and 6 show the variations of the phase velocity and coupling impedance when h_l is 0.1, 0.2, 0.4, and 0.8 cm, respectively. With the reduction of h_l, phase velocity decreases and the coupling impedance rapidly lessens.

The relations between the v_p, K_c, and f for various r_c are given in Figs. 7 and 8. It can be seen that for the same frequency the decrease of the radius r_c leads to the increase of the phase velocity and coupling impedance. The raising of K_c can be explained as follows: the field is pushed toward the gap with the reducing of r_c, therefore, the impedance increases.

The effect of width w of the gap on the phase velocity is far less than that of h_l and r_c (Figs. 9 and 10). At the moment of the high frequency, the change of w almost does not cause any variation of v_p. The coupling impedance K_c has a more complex relation with width w—the intersection of the curves obviously occurs here. However, in summary, the variation of K_c with w is not large.

VI. Summary

The detailed analysis of the ridge-loaded helical groove is presented and the dispersion equation and the expression of the coupling impedance are given. It is indicated from

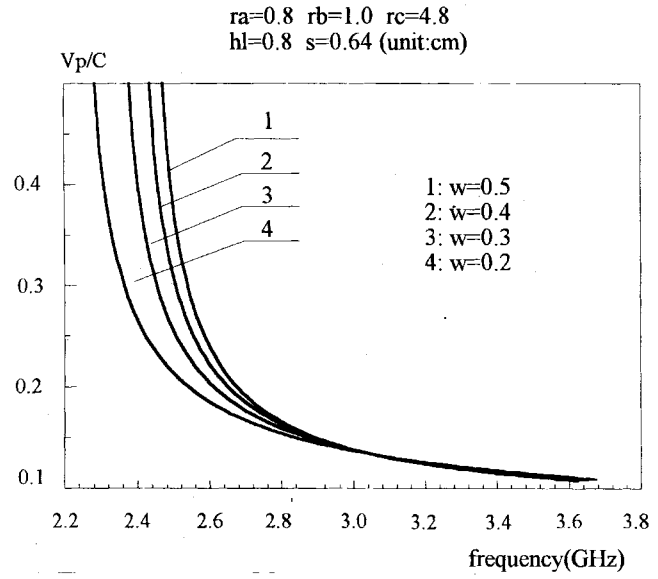

Fig. 9. The relation between the phase velocity and frequency for various w.

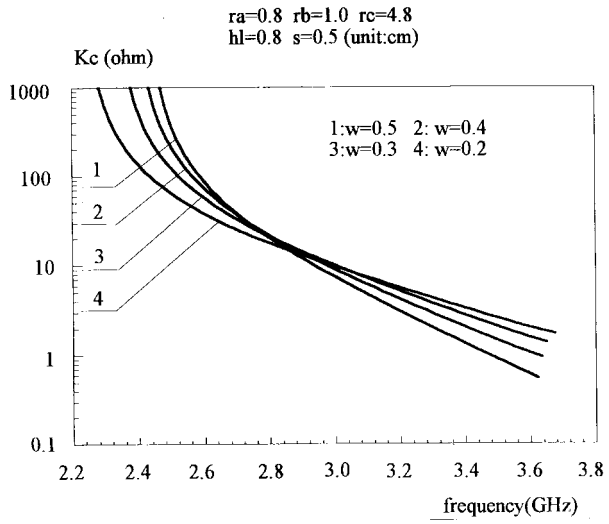

Fig. 10. The relation between the coupling impedance and frequency for various w.

the calculations that this type of slow-wave structure has approximately 30% bandwidth. The curves of the relations between the phase velocity or coupling impedance and the dimensions of the structure are also obtained. These curves are useful for designing the ridge-loaded helical-groove slow-wave structure.

REFERENCES

[1] R. A. Waldron, "Theory of the helical waveguide of rectangular cross section," *J. British IRE*, vol. 17, pp. 577–592, Oct. 1957.
[2] S. Ahn and A. K. Ganguly, "Analysis of helical waveguide," *IEEE Trans. Electron Devices*, vol. ED-33, pp. 1348–1355, Sept. 1986.
[3] L. M. Field, "Some slow-wave structure for TWT," *Proc. IRE*, vol. 37, pp. 34–40, Jan. 1949.
[4] B. T. Henoch, "Investigations of the disk-loaded and helical waveguides," *J. Appl. Phys.*, (Transl. Roy. Inst. Technol., Stockholm, Sweden), vol. 18, no. 129, pp. 1–83, May 1958.
[5] M. A. Nwachuku, "The helical waveguide as a periodic structure for millimeter wave," Ph.D. dissertation, Dept. Elect. Eng., Univ. London, London, U.K., 1961.
[6] D. I. Voskresenskii and R. A. Granovskajia, "Investigation of the type of helical-channel slow-wave system," in *Electromagnetic Slow-Wave System*. Moscow, Russia: National Defense Press, 1960, pp. 98–103.
[7] K. W. H. Foulds and J. R. Mansell, "Propagation of an electromagnetic wave through a helical waveguide," *Proc. Inst. Elect. Eng.*, vol. 111, pp. 1789–1798, Nov. 1964.
[8] C. Liss, R. Harper, and M. P. Puri, "Helical waveguide millimeter wave TWT," in *IEDM'88*, San Francisco, CA, Dec. 11–14, 1988, pp. 374–377.
[9] S. Ramo, J. Whinnery, and T. Van Duzer, *Fields and Waves in Communication Electronics*. New York: Wiley, 1965, p. 598.
[10] G. N. Watson, *A Treatise on the Theory of Bessel Functions*, 2nd ed. Cambridge, U.K.: Cambridge Univ. Press, 1994.

Wenxiang Wang was born in the province of Jiangsu, China, on July 24, 1940. He graduated from Chengdu Institute of Radio Engineering [now the University of Electronic Science and Technology of China UESTC] in 1963.

He has worked at the Institute of High Energy Electronics, UESTC, since 1963. From 1963 to 1978, he was engaged in the field of microwave electronic tubes including TWT's, CW magnetrons, forward-wave amplifiers, etc. Since 1979, his research activities have been concerned with gyrotrons, high-power microwave tubes, and techniques. From 1986 to 1988, he joined the Plasma Research Laboratory, University of Maryland at College Park, as a Visiting Scholar, where he investigated and designed the high-power mode-selective directional coupler for gyroklystron. He is currently a Professor at UESTC.

Mr. Wang is a committee member of the Chinese Vacuum Electronics Society and a senior member of the Chinese Institute of Electronics.

Guofen Yu received the B.S. degree in applied physics from the Changsha Institute of Technology, China, in 1987, the M.S. degree in electronic physics from the University of Electronic Science and Technology of China (UESTC), Chengdu, Sichuan, China, in 1990, and is currently working toward the Ph.D degree at UESTC, performing research in the field of traveling-wave tube.

Since 1990, she has been working at the UESTC, where her research interests are microwave sources such as the TWT, gyrotron, vircator, and high-power microwaves.

Yanyu Wei was born in 1971. He received the B.S. degree in nuclear electronics and application of nuclear technology from Southmiddle College of Technology, Heng-yang, China, in 1993, the M.S. degree in electronic physics from the University of Electronic Science and Technology of China (UESTC), Chengdu, Sichuan, China, in 1996, and is currently working toward the Ph.D. degree at UESTC.